Diagnostic Analysis and Spectral Energetics of a Blocking Event in the GLAS Climate Model Simulation

TSING-CHANG CHEN

Department of Earth Sciences, Iowa State University, Ames, Iowa 50011

J. SHUKLA

Laboratory for Atmospheric Sciences, NASA-Goddard Space Flight Center, Greenbelt, MD 20771

(Manuscript received 6 November 1981, in final form 12 October 1982)

ABSTRACT

We examine diagnostically the structure and spectral energetics of an amplified persistent blocking ridge and trough pattern that occurred in one of the GLAS climate simulations. This particular model simulation was performed by Shukla and Bangaru (1979) to study the sensitivity of the quasi-stationary waves to the North Pacific sea surface temperature anomalies. The spectrally filtered Hovmöller diagram shows that wavenumbers 2 and 3 in the anomaly run become *stationary* near their climatological locations. The constructive interference of wavenumbers 2 and 3 forms two persistent blocking ridges: one in the west coast of North America and the other in western Europe.

Spectral energetics analysis of this blocking case shows that A_2 and A_3, the available potential energy of wavenumbers 2 and 3, are supplied by the conversion from zonal available potential energy. K_2 and K_3, the kinetic energy of these two waves, are maintained by different processes: K_2 is maintained by conversion from A_2 to K_2, a baroclinic process, while K_3 is mainly maintained by conversion from K_Z, the zonal kinetic energy, to K_3, a barotropic process.

The model-simulated blocking episode is similar to the atmospheric circulation conditions in January 1963 and the 1976–77 winter. The spectral energetics for these two periods are compared with those of the model simulation, and in most instances, are found to be quite similar.

1. Introduction

Although the short-range day-to-day weather fluctuations in mid-latitudes are generally dominated by traveling disturbances, the occurrence of persistent anomalies associated with the phenomena of blocking are of great importance for medium- and long-range forecasting. Though global general circulation models have shown considerable success in simulating the mean climate and its variability, and fair success at short ranges, we do not know much about the ability of the climate models to simulate the geographical locations, intensity and frequency of blocking events or persistent anomalies. A preliminary examination of several simulations by the GLAS climate model has revealed that the model-generated blocking events do not persist as long or occur as frequently as actually observed. Since this model has a coarse resolution (4° latitude × 5° longitude), it cannot resolve small-scale waves. If the interactions between the blocking pattern and these waves are important for maintenance of the block, it is likely that models with more accurate treatment of these interactions (*viz.* high-resolution models) will simulate the blocking phenomena more realistically. This notion is supported in a case study by Bengtsson (1981). However, under certain conditions, the GLAS climate model atmosphere is observed to develop blocks. It is then of interest to examine the energetics of these specific episodes in the hope we can further understand those processes which establish and maintain persistent anomalies.

Shukla and Bangaru (1979) carried out a numerical experiment to study the sensitivity of the GLAS model to SST anomalies in the North Pacific. They integrated the model with SST anomalies which had a spatial structure similar to the one observed in January 1977. It was one of a few cases which showed a realistic simulation of a persistent blocking ridge. Therefore, it suggests the possible role of diabatic heat sources associated with the large-scale SST anomalies in the generation of blocking events.

In this paper we discuss the synoptic and spectral analysis of this blocking event. We examine the time evolution, maintenance and decay of the block by studying the energetics and energy conversion processes, and compare them to similar analyses of atmospheric blocking episodes. In addition, we also make limited use of a control run in which the GLAS climate model was integrated with no SST anomaly and exhibited no large-amplitude block.

Our study proceeds as follows: A brief description

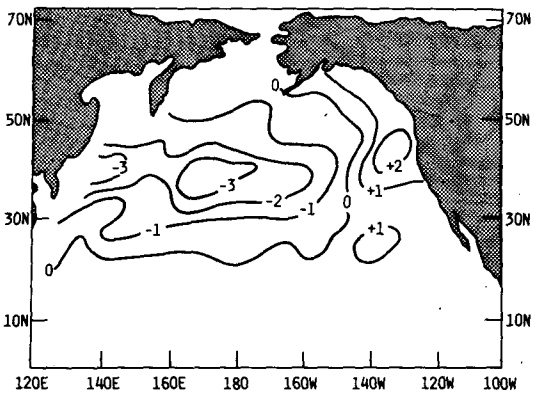

FIG. 1. The sea surface temperature (SST) anomaly (°C) used in the anomaly run. The structure of this SST anomaly is the same as that observed by Namias (1978) but of greater amplitude by a factor of 9/5.

of the GLAS model and the numerical experiments as carried out by Shukla and Bangaru is provided in Section 2. Section 3 discusses the synoptic and spectral analyses of the experiments and the formation of the persistent blocking ridges. Section 4 presents the spectral energetics of the planetary waves which appear to maintain the blocking ridge. In Section 5, we compare the spectral energetics of the model simulations with actual observations. A summary is presented in Section 6.

2. Description of the GLAS general circulation model and experimental design

a. Model

The general circulation model used in this study is the second-order version of the Goddard Laboratory for Atmospheric Sciences (GLAS) climate model described by Halem *et al.* (1979). The model is a global primitive-equation model which is developed in the sigma vertical coordinate system with nine levels between the surface and the top at 10 mb. The horizontal grid spacing is 4° latitude and 5° longitude. A variable horizontal grid with coarser spacing near the pole is introduced.

The model also includes a detailed parameterization of sub-grid-scale processes. Two different mechanisms, large-scale supersaturation and parameterized moist convection, are used to generate condensation and cloud. Longwave and shortwave radiative heating are calculated at 5 h intervals. The ground temperature is calculated from the net heating and cooling at the surface by radiation, sensible heat and latent heat fluxes. The geographical distribution of albedo, ice and snow cover are specified. The soil moisture is a predicted variable. Sea surface temperatures are updated daily from the observed climatological values by a linear interpolation between the midpoints of two consecutive months.

b. Numerical experiments

In the winter of 1976–77, severe weather occurred over North America. Extreme cold dominated the eastern part of the United States and record drought affected the far west. In addition, abnormal warmth occurred over Alaska and much of the Canadian Arctic. Namias (1978) examined the possible causes of this severe winter weather and found that the North Pacific sea surface temperatures were abnormally cold in the northern and western sections, and abnormally warm off the west coast of the United States (Fig. 1). Namias suggested that these SST anomalies might have been one of the multiple causes of the abnormally cold temperatures in eastern North America during the winter of 1976–77.

Shukla and Bangaru (1979) carried out a numerical experiment with the GLAS climate model to test Namias' hypothesis. The experiments were performed by first integrating the GLAS model for 60 days with the climatological mean SST and the observed initial conditions for 1 January 1975. This integration is referred to as the *control run.* The slowly varying climatological SST field was then changed by superposing a time-invariant SST anomaly field upon this climatological field. The distribution of the imposed SST anomaly is shown in Fig. 1. The spatial structure of the SST anomaly is the same as that ob-

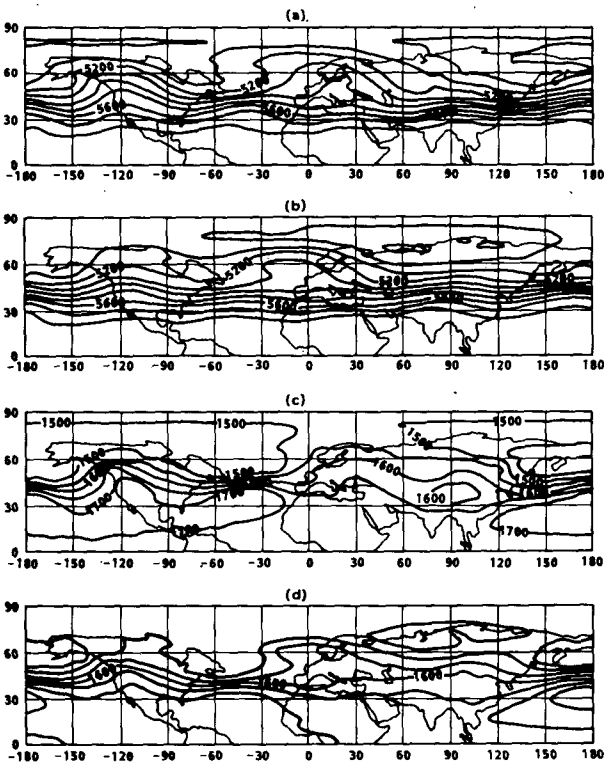

FIG. 2. Two-week (1–14 February) mean height fields (m): (a) 500 mb anomaly run, (b) 500 mb control run, (c) 850 mb anomaly run, and (d) 850 mb control run.

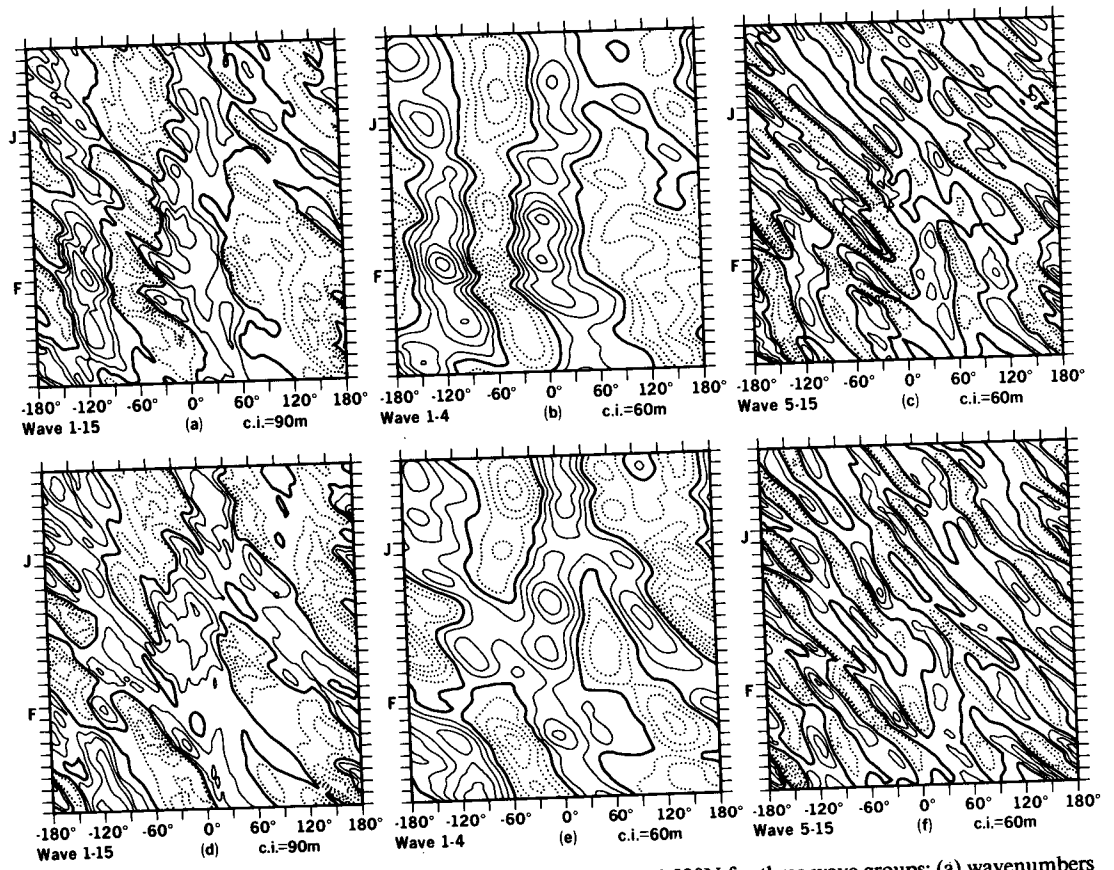

FIG. 3. Spectrally filtered Hovmöller diagrams (m) at 500 mb and 50°N for three wave groups: (a) wavenumbers 1–15 of anomaly run, (b) wavenumbers 1–4 of anomaly run, (c) wavenumbers 5–15 of anomaly run, (d) wavenumbers 1–15 of control run, (e) wavenumbers 1–4 of control run, and (f) wavenumbers 5–15 of control run. Dotted contours are negative values.

served by Namias (1978) but of greater amplitude by a factor of 9/5. The model was then integrated again with the same initial conditions as the control run but with the anomalous values of the SST for 60 days and will be referred to as the *anomaly run*. Since this is not a coupled ocean–atmosphere model, SST anomalies are assumed to persist for the whole period of integration. This assumption is justified by the fact that SST anomalies are observed to persist for a period of several months (Namias, 1970) which is considerably longer than the integration period. The purpose of Shukla and Bangaru's numerical experiment was not to simulate the actual events of the 1976–77 winter but to examine the effects of similar SST anomalies on the model atmosphere. Although the primary objective of this study is to diagnose the resulting model-simulated blocking, we have also presented some results of the control run for comparison.

3. Synoptic and spectral analysis

a. Synoptics

The examination of model daily charts (not shown) for the first two weeks of February of both runs reveals that a two ridge-trough system over western North America and western Europe always exists, but the features in the anomaly run were consistently of higher amplitude and more persistent. In order to have an overview of the synoptic difference between these two runs, the mean height fields for these two weeks at 500 and 850 mb are shown in Fig. 2.

The two-week mean height fields of both anomaly and control runs at 500 mb are characterized by two ridge-trough systems. In fact, this feature of the circulation pattern is also perserved in both runs at 850 mb. Two ridges exist over the west coast of North America and western Europe. It is of interest to note that the trough and ridge lines tilt from southeast to northwest. This type of synoptic structure implies the southward eddy transport of momentum (Starr, 1948). The difference between the anomaly and control runs is that the troughs and ridges are amplified significantly in the former run. In addition, the ridge of the anomaly run over western Europe is shifted westward at 500 mb and eastward at 850 mb with respect to that of the control run. This contrast between both runs is especially pronounced north of 60°N.

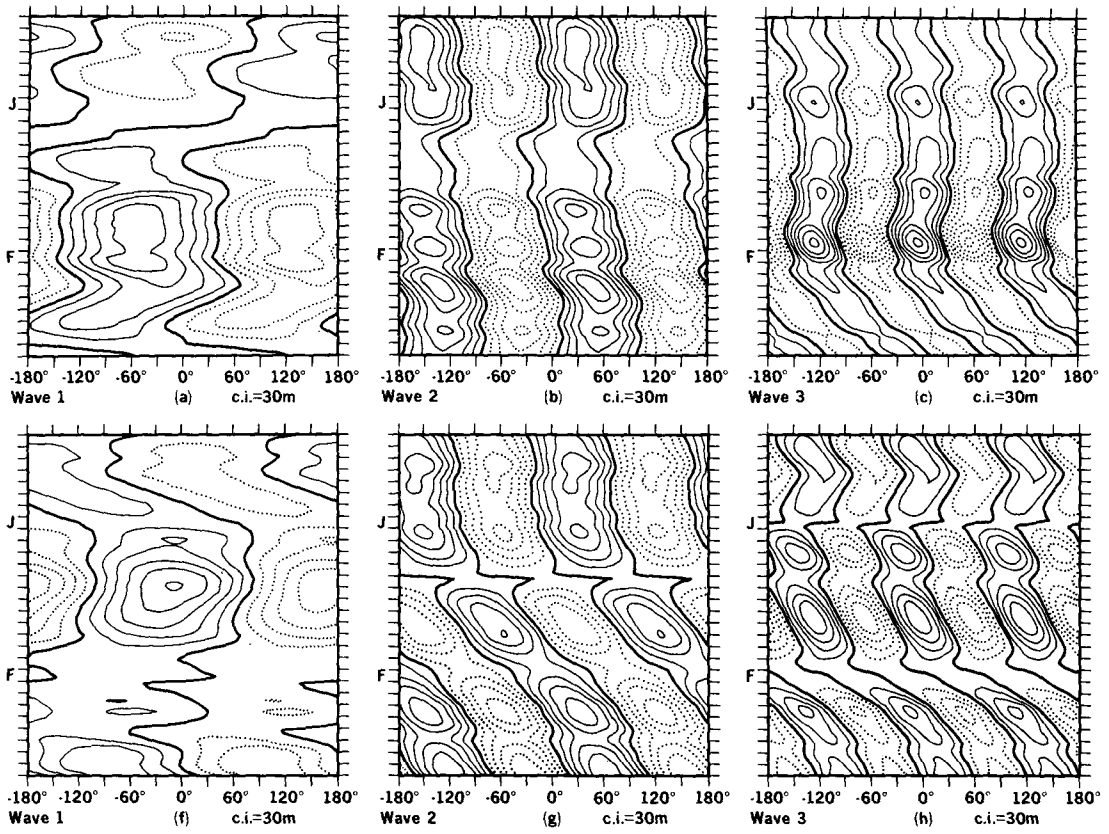

FIG. 4. Spectrally filtered Hovmöller diagrams (m) at 500 mb and 50°N for the first four wavenumbers and combination of wavenumbers 2 and 3. (a)–(e) are anomaly runs, while (f)–(j) are control runs.

The deepening of the low (or trough) over the Pacific and the intensification of the ridge over the west coast of North America are the most striking features of the anomaly run.

b. Spectral analysis

The comparison of the time-mean height fields between both runs clearly reveals that the most distinguishable difference is in the large-scale features. In other words, the major response in the time mean of the GLAS model atmosphere to the SST anomalies over the North Pacific appears to be in the long waves. To better display the time-dependent behavior of the model response, we examine the Hovmöller's (1949) diagrams for the spectrally filtered (SF) height fields at 500 mb at 50°N. Fig. 3 shows these diagrams for three different wave groups: wavenumbers 1–15, wavenumbers 1–4 and wavenumber 5–15. The first wave group is regarded as the total wave disturbance, the second wave group as the long waves, and the third wave group as the short waves.

The SF Hovmöller diagrams of wavenumbers 1–15 for both the anomaly and control runs (Figs. 3a and 3d) show that two ridge-trough systems exist over most of the simulation period. The trough-ridge system in the anomaly run is much more persistent, while it has a tendency to propagate eastward in the control run. Closer examination of Figs. 3a and 3d reveals that the trough-ridge systems of both runs during the third week of January (just prior to the establishment of the blocking episode in the anomaly run) are still quite similar. This may indicate that the model retains some memory of the initial height field or, perhaps, that the response to the SST is quite slow.

In order to examine the role played by the long- and short-wave components, the SF Hovmöller diagrams of wavenumbers 1–4 and 5–15 are also displayed in Figs. 3b, 3c, 3e, and 3f, respectively. The comparison between the long-wave SF Hovmöller diagrams and the total wave SF Hovmöller diagrams shows very clearly that the large-scale pattern of the ridge-trough system in both runs is explained primarily by the long-wave components. Consequently, the persistent blocking ridges in the model anomaly run appear to be a result of the long waves becoming stationary and amplifying.

The short-wave SF Hovmöller diagrams characterize the eastward propagation of the short waves over most of the longitudes and time. However, the

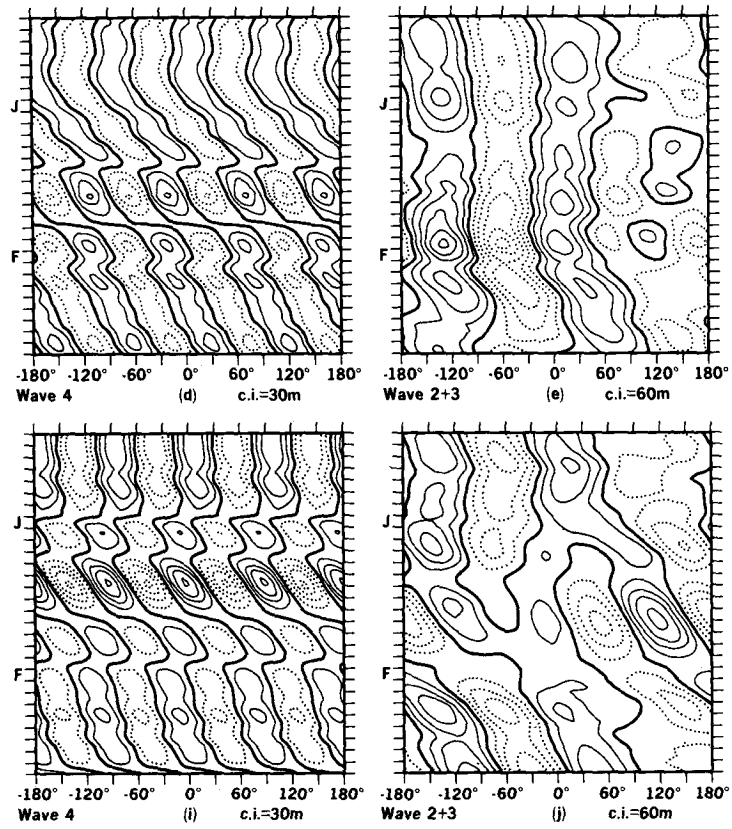

FIG. 4. (*Continued*)

short waves of both the control and anomaly runs have stationary ridges located at 30°E in the first two weeks of February. In addition, the troughs and ridges of the short-wave components in the anomaly run between 60°E and 120°W are also quasi-stationary. The quasi-stationarity in the short waves of the anomaly run seems to be associated with the blocking episode.

To further analyze the large-scale structure of the model runs, the SF Hovmöller diagrams for each individual long wave from wavenumber 1 to 4 are depicted in Fig. 4. The most pronounced difference between the two runs are wavenumbers 2 and 3. These two waves "lock in" the anomaly run. It is also interesting to note that the superposition of wavenumbers 2 and 3 (Fig. 4e) provides a reasonable kinematic explanation for the two persistent blocking ridges, shown in Figs. 2a or 2b.

The synoptic structure of wavenumbers 2, 3, and combinations of them at 1200 GMT 4 February is illustrated in Fig. 5. Shown are 500 mb height and temperature. The highs of wavenumber 2 are located at Alaska Bay and north central Europe, while those of wavenumber 3 are anchored at the west coast of Canada, the North Sea and Siberia. The combination of these two waves forms two highs at the west coast of Canada and the North Sea with a deep low located at Labrador and another broad low extending from north Africa to the northwestern Pacific. The pattern formed by the combination of temperature waves 2 and 3 is very similar to the pattern formed by height waves 2 and 3, except the warmest temperature centered at Alaska Bay is shifted westward with respect to the high of the height field. The comparison of individual waves of height and temperature shows that wavenumber 2 has a significant phase lag between height and temperature and wavenumber 3 does not. In fact, the observations of daily spectral analyses reveal that the wavenumber 2 height field leads the wavenumber 2 temperature from 10 to 30° longitude. On the contrary, the height and temperature field of wavenumber 3 do not show any significant phase lag. This observation indicates that wavenumber 2 is baroclinic and wavenumber 3 is essentially barotropic. The remarkable structural differences between these two waves must be related to the differences between the physical processes which develop and maintain them.

4. Energetics

a. Energetics scheme

The development and maintenance of the blocking ridges will be illustrated in terms of Saltzman's (1957)

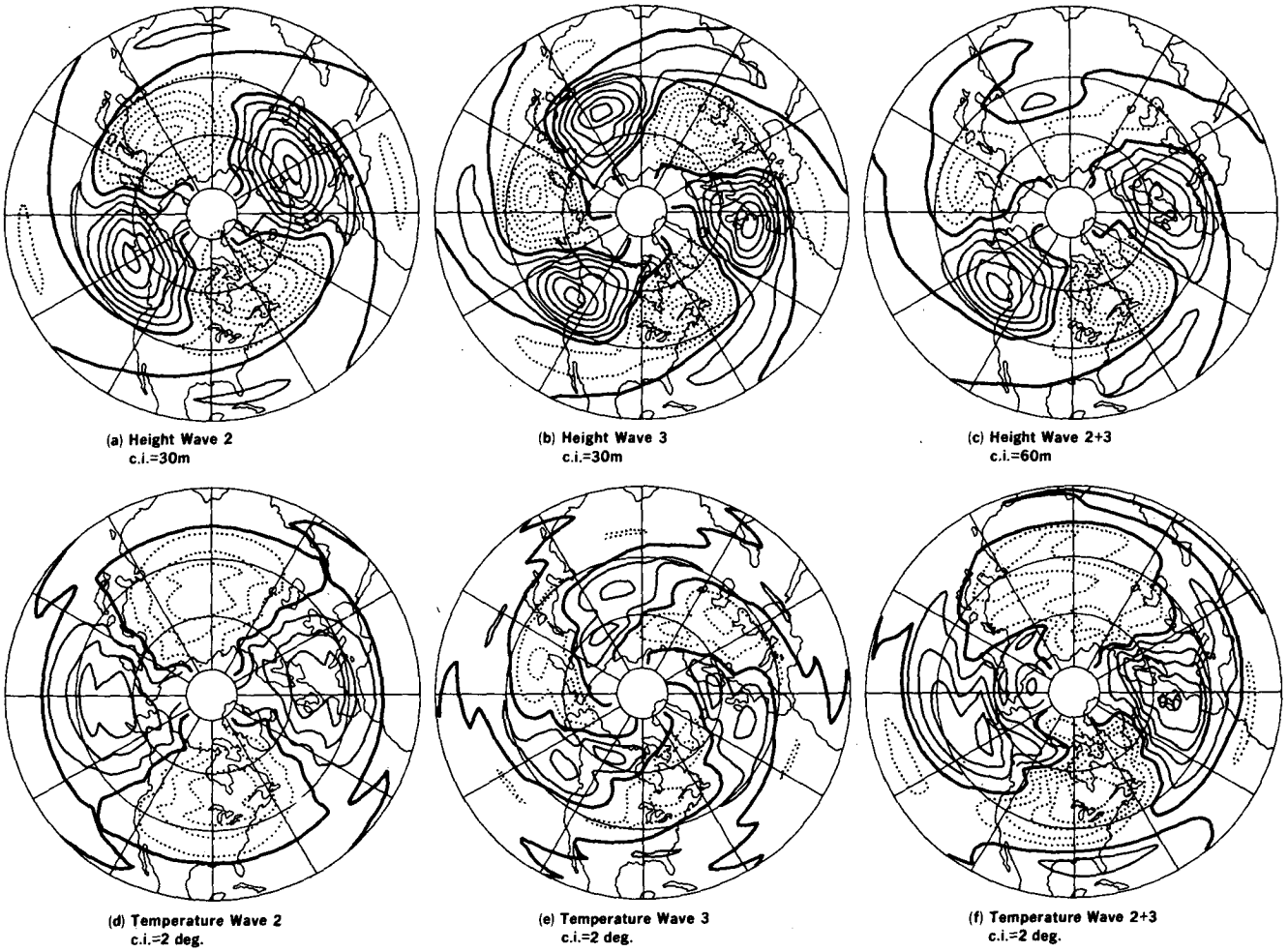

FIG. 5. Spectrally filtered synoptic charts of height (m) and temperature (°C) of anomaly run for wavenumber 2, 3 and combinations of them at 500 mb on February 4.

spectral energetics scheme employed over latitude zone 26–86°N. This spectral energetics scheme is also used in our recent studies (Chen, 1982; Hansen and Chen, 1982). Following Saltzman's formulation and Steinberg *et al.*'s (1971) expression, the spectral energy equations in symbolic form can be written as

$$\frac{dK_Z}{dt} = \sum_{n=1}^{N} C(K_n, K_Z) + C(A_Z, K_Z) + F(K_Z) - D(K_Z), \quad (1)$$

$$\frac{dK_n}{dt} = -C(K_n, K_Z) + CK(n|m, l) + C(A_n, K_n) + F(K_n) - D(K_n), \quad (2)$$

$$\frac{dA_Z}{dt} = -\sum_{n=1}^{N} C(A_Z, A_n) - C(A_Z, K_Z) + F(A_Z) + G(A_Z), \quad (3)$$

$$\frac{dA_n}{dt} = C(A_Z, A_n) - C(A_n, K_n) + CA(n|m, l) + F(A_n) + G(A_n), \quad (4)$$

where K and A represent kinetic and available potential energy. The subscripts Z and n denote zonal and wave components. The rate of change of various energy components on the left-hand side is determined by the various energetic processes on the right-hand side. $C(P, Q)$ represents the energy conversion from P to Q. Note that

$$\sum_{n=1}^{N} C(K_n, K_Z) = C(K_E, K_Z)$$

and

$$\sum_{n=1}^{N} C(A_Z, A_n) = C(A_Z, A_E).$$

$CX(n|m, l)$ is the gain rate to wavenumber n of quan-

tity x due to triplet interactions between all possible combinations of m and l with n. $F(x)$ gives the contribution due to the flux across the lateral boundary of the open region. $G(A)$ and $D(K)$ are generation of available potential energy and dissipation of kinetic energy, respectively.

Equations for eddy energies

$$K_E = \sum_{n=1}^{N} K_n \quad \text{and} \quad A_E = \sum_{n=1}^{N} A_n$$

can be obtained by summing (2) and (4) from $n = 1$ to N, i.e.,

$$\frac{dK_E}{dt} = -C(K_E, K_Z) + C(A_E, K_E) + F(K_E) - D(K_E), \quad (5)$$

$$\frac{dA_E}{dt} = C(A_Z, A_E) - C(A_E, K_E) + F(A_E) + G(A_E). \quad (6)$$

The traditional Lorenz energy cycle consists of Eqs. (1), (3), (5) and (6).

b. *Overview of model energetics during blocking events*

Time variations of various energies [A_Z, A_E, K_Z and K_E] and various energy conversions [$C(A_Z, A_E)$, $C(A_E, K_E)$ and $C(K_E, K_Z)$] from 16 January to 14 February in the anomaly run are depicted in Figs. 6a–6c. The amplification of blocking ridges located on the west coast of North America and western Europe in the anomaly run occurs during the first two weeks of February. Figs. 6a and 6b show that A_Z and K_Z start to decline on 30 January , while A_E and K_E increase. Then, A_E and K_E, especially the latter, decrease around 7 February, and both increase again about 10 February. Notice that both A_Z and K_Z increase, in general, when A_E and K_E decrease, or vice versa.

The energy conversions $C(A_Z, A_E)$ and $C(A_E, K_E)$ are always positive. In addition, their time variations are consistent with the time variations of A_E and K_E. It should be noted that $C(K_E, K_Z)$ is negative over most of the time period in the anomaly run. This indicates that both barotropic and baroclinic processes are important for the maintenance of the eddy disturbances.

Winston and Krueger (1961) and Miyakoda (1963) examined the time variations of A_Z, A_E, K_Z and K_E and Paulin (1970) calculated the time variations of various energy conversions during the blocking events. Based upon the results of these studies, Lejenas (1977) produced a schematic picture (Fig. 7) of the energy changes and energy conversions during a blocking episode. The arrows indicate the directions of various energy conversions and at which time they reach their maxima. The energetics during the development of the model blocking depicted in Figs. 6a and 6b show a very striking similarity to Lejenas' schematic picture.

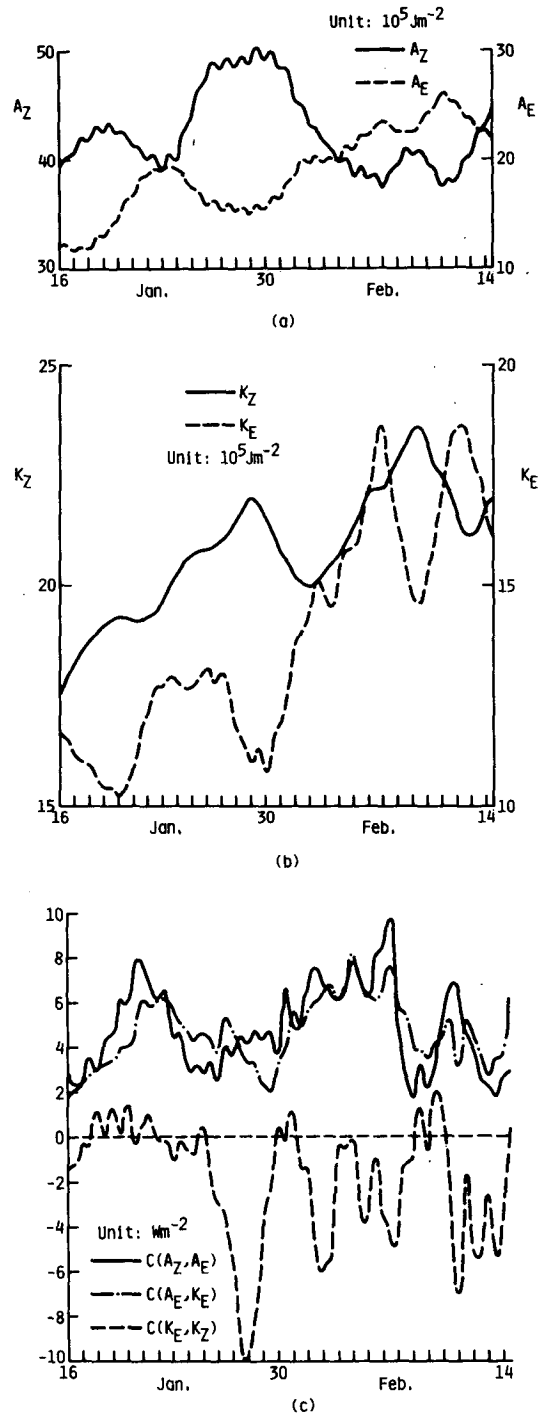

FIG. 6. Time variations of energies: (a) A_Z and A_E, (b) K_Z and K_E, and (c) energy conversions $C(A_Z, A_E)$, $C(A_E, K_E)$ and $C(K_E, K_Z)$.

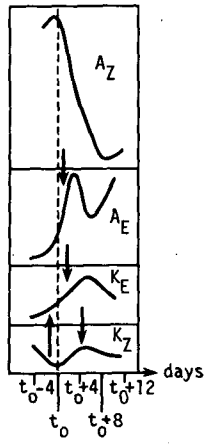

FIG. 7. Schematic picture of the energy changes and energy conversions during a blocking situation. Day $t = t_0$ is the onset of the blocking (after Lejenäs, 1977).

c. *Dynamical transports of wavenumbers 2 and 3 during blocking*

It was noted in Section 3 that the life period of the blocking ridges generated in the anomaly run was about two weeks. The spectral analysis in Section 3 showed that the formation of the blocking ridges was essentially due to the constructive interference of wavenumbers 2 and 3. We have examined the spectral energetics and dynamical transports of these two waves to understand the maintenance of blocking ridges.

Fig. 8 depicts the time variation of the zonal flow and temperature at 500 mb for the anomaly run. The zonal flow between 26 and 82°N starts to decrease when the blocking ridges develop at the end of January. The zonal flow increases again after about 4 days. An interesting feature about the zonal flow is the weakening of westerlies in high latitudes (60–70°N) from 3–9 February. This is perhaps due to the warming at high latitudes shown in Fig. 8b. Therefore, the north–south temperature gradient is reduced and, in turn, the zonal wind is decreased according to the thermal wind relationship. This warming may be caused by the northward transports of sensible heat by waves 2 and 3 which are amplified very significantly during the formation of the blocking ridges.

The time variations of momentum and sensible heat transports[1] by wavenumbers 2 and 3, $\overline{u'v'}(2)$, $\overline{v'T'}(2)$, $\overline{\omega'T'}(2)$, $\overline{u'v'}(3)$, $\overline{v'T'}(3)$ and $\overline{\omega'T'}$, are displayed in Fig. 9. It can be seen that momentum and sensible heat transports by wavenumbers 2 and 3 occur mainly in high latitudes. This is consistent with the observational spectral analysis of these two transports by Wiin-Nielsen *et al.* (1964). Note that $\overline{u'v'}(2)$ and $\overline{u'v'}(3)$ are, in general, southward in high latitudes while $\overline{v'T'}(2)$ and $\overline{v'T'}(3)$ are northward. There are, however, some noteworthy exceptions. For example, $\overline{u'v'}(3)$ becomes significantly northward from mid-latitudes to high latitudes during the mature stage of the block, and $\overline{v'T'}(3)$ reverses sign and becomes significantly southward for a brief period during the developing stage of the block. This indicates that $\overline{v'T'}(2)$ alone is principally responsible for the warming in high latitudes shown in Fig. 8, which is consistent with our observation that wavenumber 2 is highly baroclinic in nature. Furthermore, the vertical heat transports $\overline{\omega'T'}$ which are proportional to the baroclinic energy conversions between A_E and K_E, possess substantial amplitudes only in the $\omega'T'(2)$ components. These behaviors strongly support our notion that wavenumber 2 is significantly more baroclinic than wavenumber 3.

The blocking ridges shown in Fig. 2 reach their maximum intensity on 4 February. The geographic distributions of $\overline{u'v'}$, $\overline{v'T'}$ and $\overline{\omega'T'}$ of wavenumbers 2 and 3, and sum of these two waves at 500 mb on 4 February are also shown in Fig. 10. Inspection of these figures reveals that the momentum transport of wavenumber 3 dominates that of wavenumber 2,

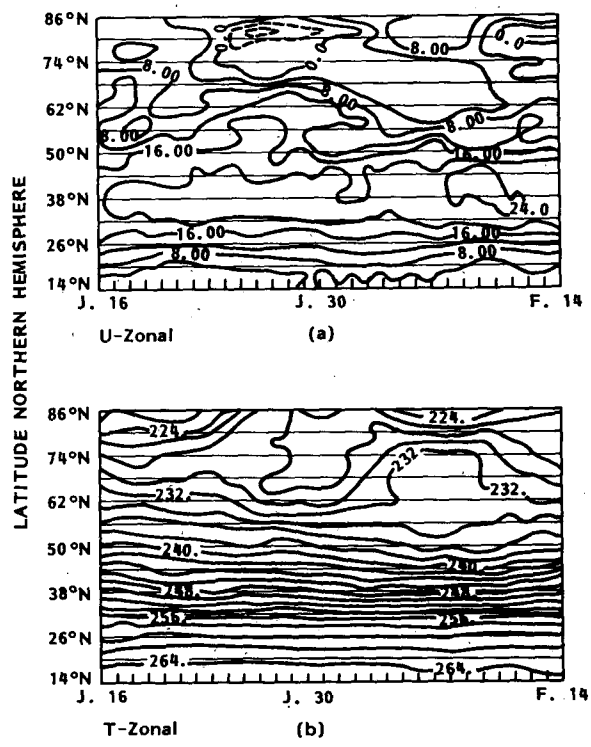

FIG. 8. Time variation of (a) zonal flow (m s^{-1}) and (b) zonal temperature (°C) at 500 mb for the anomaly run.

[1] $\overline{v'T'}(n)$, $\overline{\omega'T'}(n)$ and $\overline{u'v'}(n)$ will be used hereafter to denote, respectively, the horizontal and vertical sensible heat, and momentum transport by wavenumber n. Likewise, the contribution from two waves, e.g., 2 and 3, will be denoted by $\overline{v'T'}(2+3)$, $\overline{\omega'T'}(2+3)$ and $\overline{u'v'}(2+3)$. $(\bar{\ })$ = zonal average and $(\ )' = (\ ) - (\bar{\ })$.

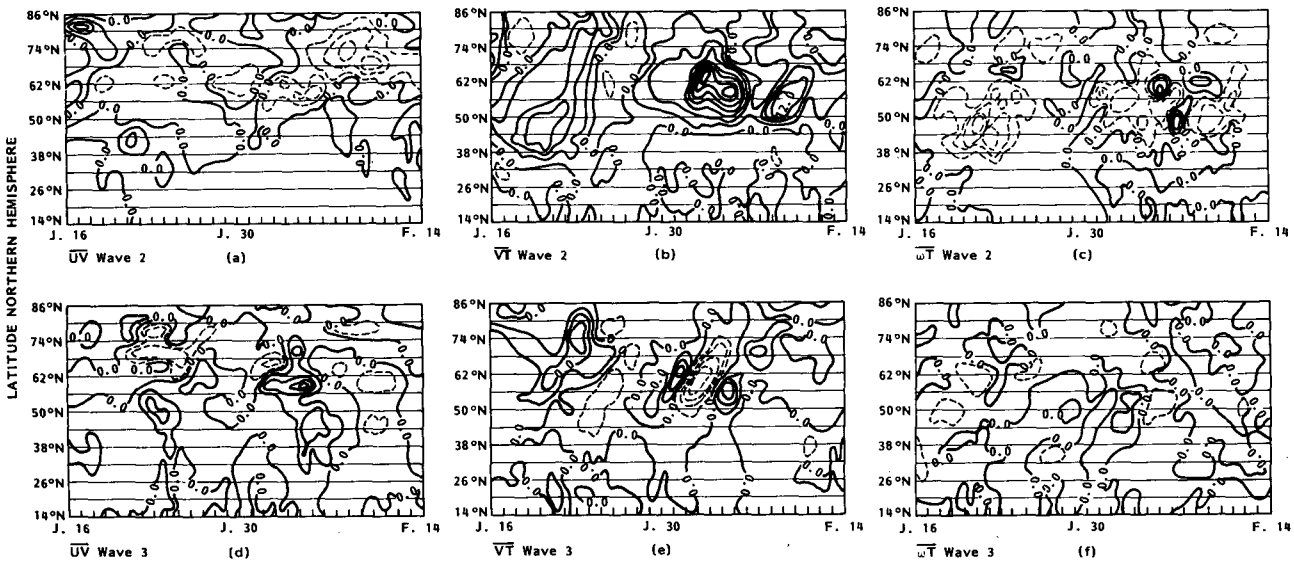

FIG. 9. Time variation of the dynamic transport by wavenumber 2, (a) $\overline{u'v'}(2)$ (b) $\overline{v'T'}(2)$, (c) $\overline{\omega'T'}(2)$, and by wavenumber 3, (d) $\overline{u'v'}(3)$, $\overline{v'T'}(3)$ and $\overline{\omega'T'}(3)$ at 500 mb for the anomaly run. Units: $\overline{u'v'}$ ($m^2\ s^{-2}$), $\overline{v'T'}$ (m °C s^{-1}), and $\overline{\omega'T'}$ (10^{-3} °C mb s^{-1}). Dotted contours are negative values.

while the reverse is true for the sensible heat transports. This contrast of transport properties between wavenumbers 2 and 3 is also consistent with the synoptic analysis that wavenumber 2 is baroclinic and wavenumber 3 is relatively barotropic. The individual sums of the transports by the two waves are a maximum in the western hemisphere. It is interesting to note that $\overline{v'T'}(2+3)$ and $\overline{\omega'T'}(2+3)$ show three areas of large value: eastern Pacific, North America and eastern Atlantic. The distribution of $\overline{v'T'}(2+3)$ can be explained by superposing the height and temperature geographic distributions of the combination of wavenumbers 2 and 3, shown in Fig. 5. Positive $\overline{v'T'}(2+3)$ over the eastern Pacific and eastern Atlantic is due to the northward advection of warm air, while positive $\overline{v'T'}(2+3)$ over North America is a result of the southward advection of cold air. $-\overline{\omega'T'}$ represents the vertical transport of sensible heat which usually is in phase with $\overline{v'T'}$.

d. Spectral energetics of wavenumbers 2 and 3

A_n and K_n of the various long waves in the anomaly run (as a function of time) are shown in Fig. 11. The inclusion of wavenumbers 1 and 4 is to provide a comparison of the energy contents in the different long waves. Although A_1 is dominant over most of February, the SF Hovmöller diagrams show that the spatial structure of the persistent blocking ridges is due mainly to the constructive interference of wavenumbers 2 and 3. Note that both A_n and K_n for wavenumbers 2 and 3 increase from the end of January when the persistent blocking ridges, shown in Fig. 2, start to develop. Further evidence demonstrating the importance of these two wavenumbers in the establishment of the block can be shown by computing the magnitudes of the various conversion terms in the Lorenz energy cycle.

We first examine the energetics of wavenumber 2 shown in Fig. 12a. A_2 is maintained by $C(A_Z, A_2)$, $C(A_2, K_2)$ and $CA(2|m, l)$. Both $C(A_Z, A_2)$ and $C(A_2, K_2)$ are positive over the time period of interest in our analysis. In other words, the energy is always converted from A_Z to A_2 and then from A_2 to K_2. Furthermore, the time variation of $C(A_Z, A_2)$ and $C(A_2, K_2)$ are in concert with that of A_2. This in-phase variation indicates that A_2 is generated by $C(A_Z, A_2)$, but is depleted by $C(A_2, K_2)$. The nonlinear interaction $CA(2|m, l)$ also extracts energy out of A_2 over most of the blocking period.

K_2 is maintained by $C(A_2, K_2)$, $C(K_2, K_Z)$ and $CK(2|m, l)$. $C(A_2, K_2)$ is found to indicate that A_2 is always converted to K_2. The sign of $C(K_2, K_Z)$ shows K_2 is principally converted to K_Z except in the second week of February. It is of interest to recall that $C(K_E, K_Z)$, shown in Fig. 6, has the opposite sense of $C(K_2, K_Z)$, which displays that K_E in the anomaly run is usually maintained by conversion from K_Z. $CK(2|m, l)$ is generally negative except when $C(A_2, K_2)$ drops significantly during 8–9 February. It is summarized that K_2 is supplied by the baroclinic energy conversion $C(A_2, K_2)$, and is depleted by the barotropic energy conversion $C(K_2, K_Z)$ and nonlinear transfers $CK(2|m, l)$.

$C(A_Z, A_2)$ and $C(A_2, K_2)$ involve the baroclinic processes of horizontal and vertical sensible heat transport, respectively, while $C(K_2, K_Z)$ is due to the barotropic process of momentum transport. The

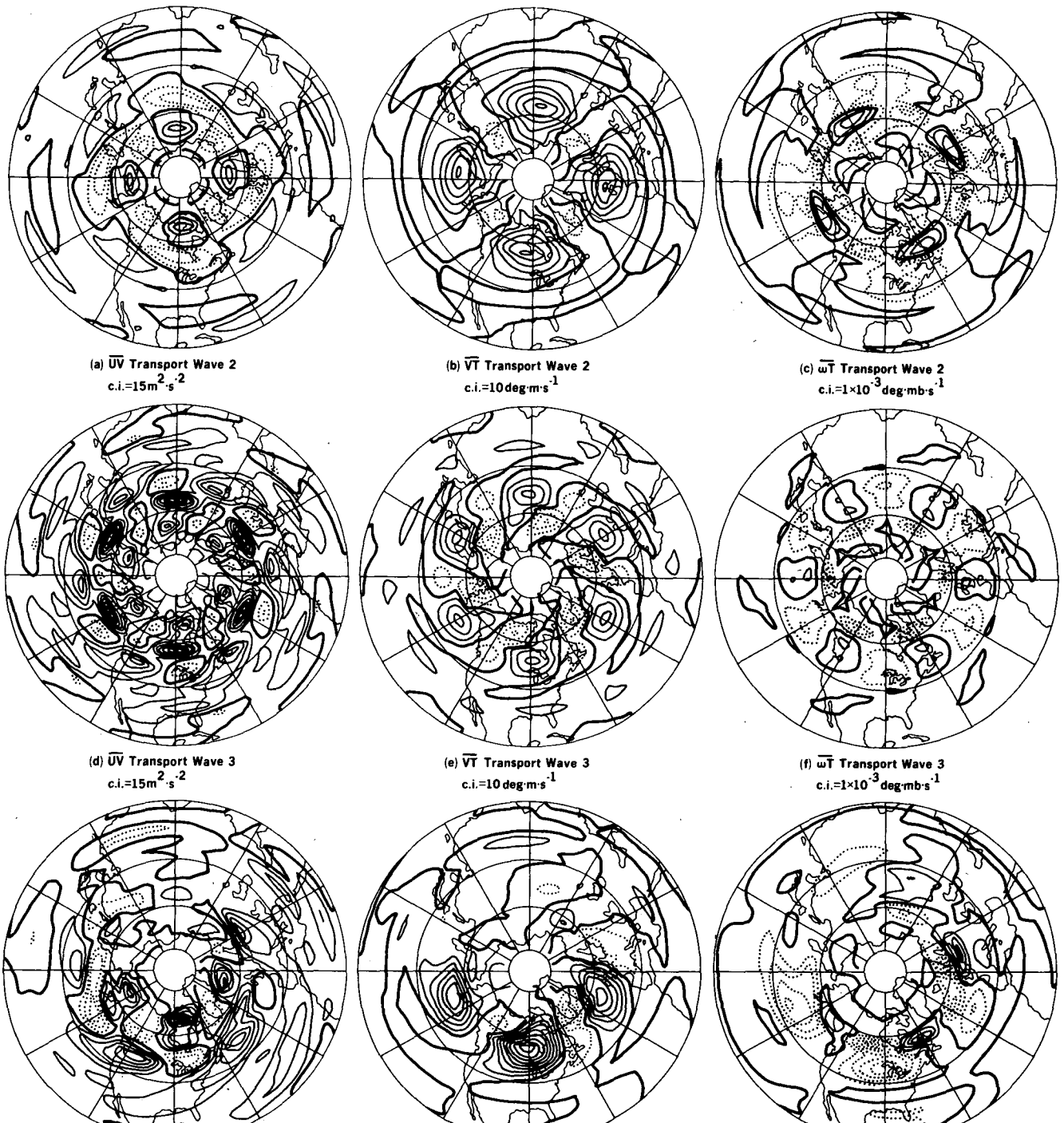

FIG. 10. Geographic distribution of $\overline{u'v'}$, $\overline{v'T'}$ and $\overline{\omega'T'}$ for wavenumbers 2, 3 and combination of them at 500 mb on 4 February. Units: as in Fig. 9.

maintenance of A_2 and K_2 is provided by $C(A_Z, A_2)$ and $C(A_2, K_2)$, respectively. This is consistent with the synoptic analysis in Section 3 which showed that wavenumber 2 temperature always has a phase lag behind wavenumber 2 height. These observations indicate that the development and maintenance of wavenumber 2 is due to the *baroclinic process.*

The time variations of various energy conversions

which maintain A_3 and K_3 are depicted in Fig. 12b. It was shown in Fig. 11b that A_3 does not increase compared with A_1 and A_2 during the development of blocking ridges, but K_3 increases to a certain extent. $C(A_Z, A_3)$ and $CA(3|m, l)$ are major sources to support A_3. However, Fig. 12b shows that the values of these two energy conversions are not significant during the development of the blocking ridges. Furthermore, the magnitude of $C(A_3, K_3)$ is not large, either. K_3 is essentially maintained by $-C(K_3, K_Z)$, the barotropic conversion releasing the available zonal kinetic energy. It is clear that the physical processes which maintain the energetics of K_3 are different from those of K_2. As we discussed in Section 3, wavenumber 3 height and temperature do not show any significant phase lag. In addition, the momentum transport of wavenumber 3 becomes very significant during the development of the blocking episode. In any event,

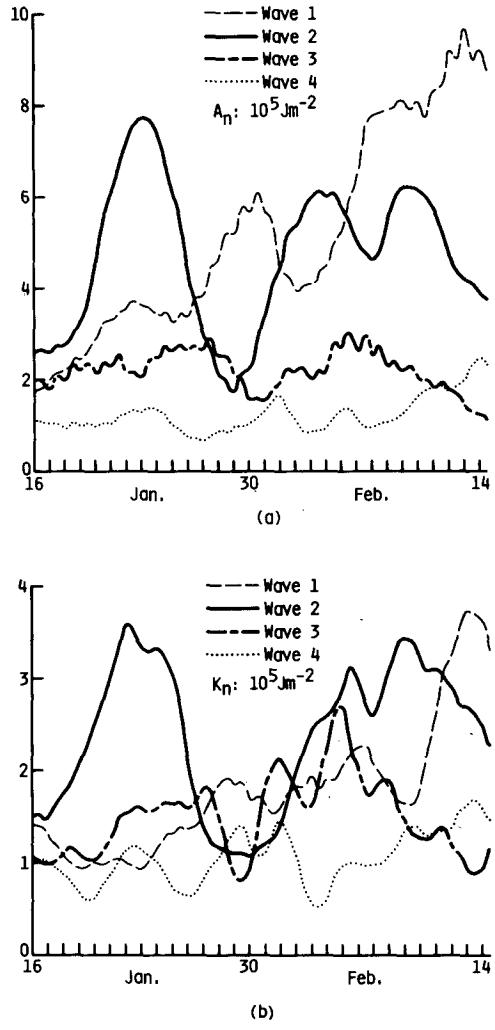

FIG. 11. Time variation of (a) available potential energy and (b) kinetic energy for wavenumber 1, 2, 3 and 4 in the anomaly run.

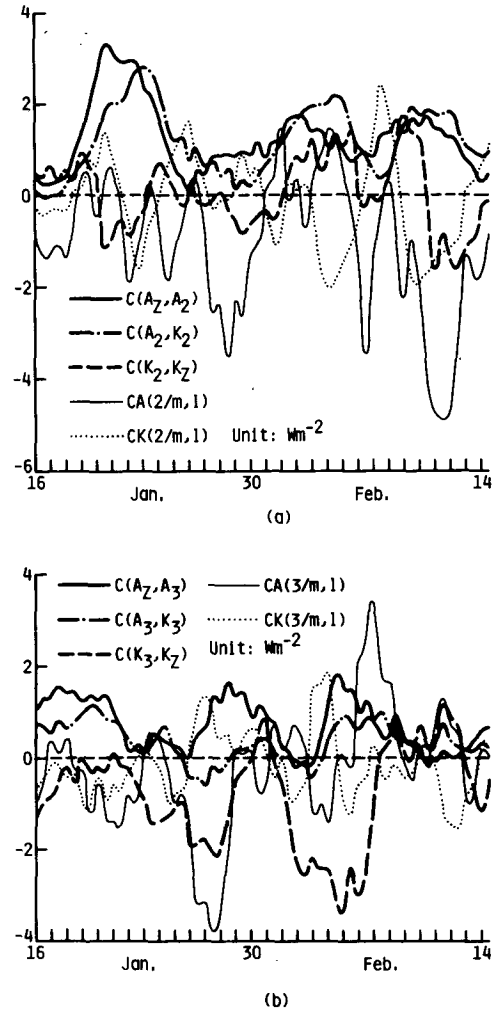

FIG. 12. Energy conversions of (a) wavenumber 2 and (b) wavenumber 3 in the anomaly run.

the above description suggests that wavenumber 3 is largely maintained *barotropically* during the existence of blocking ridges in the anomaly run.

5. Comparison with observational studies

It was pointed out by Tung and Lindzen (1979) that the United States experienced very similar abnormal circulation patterns and severe winter conditions in January 1963 and January 1977; a persistent and enormously amplified ridge existed in the eastern Pacific. The spectral energetics of the anomaly run during the existence of the persistent blocking ridges is similar to that of January 1963 which was analyzed to a great extent by Wiin-Nielsen *et al.* (1964) and Murakami and Tomatsu (1965). The comparison of the present analysis of the anomaly run with these two winters may shed some light on the physical mechanisms which cause and maintain the persistent blocking ridges.

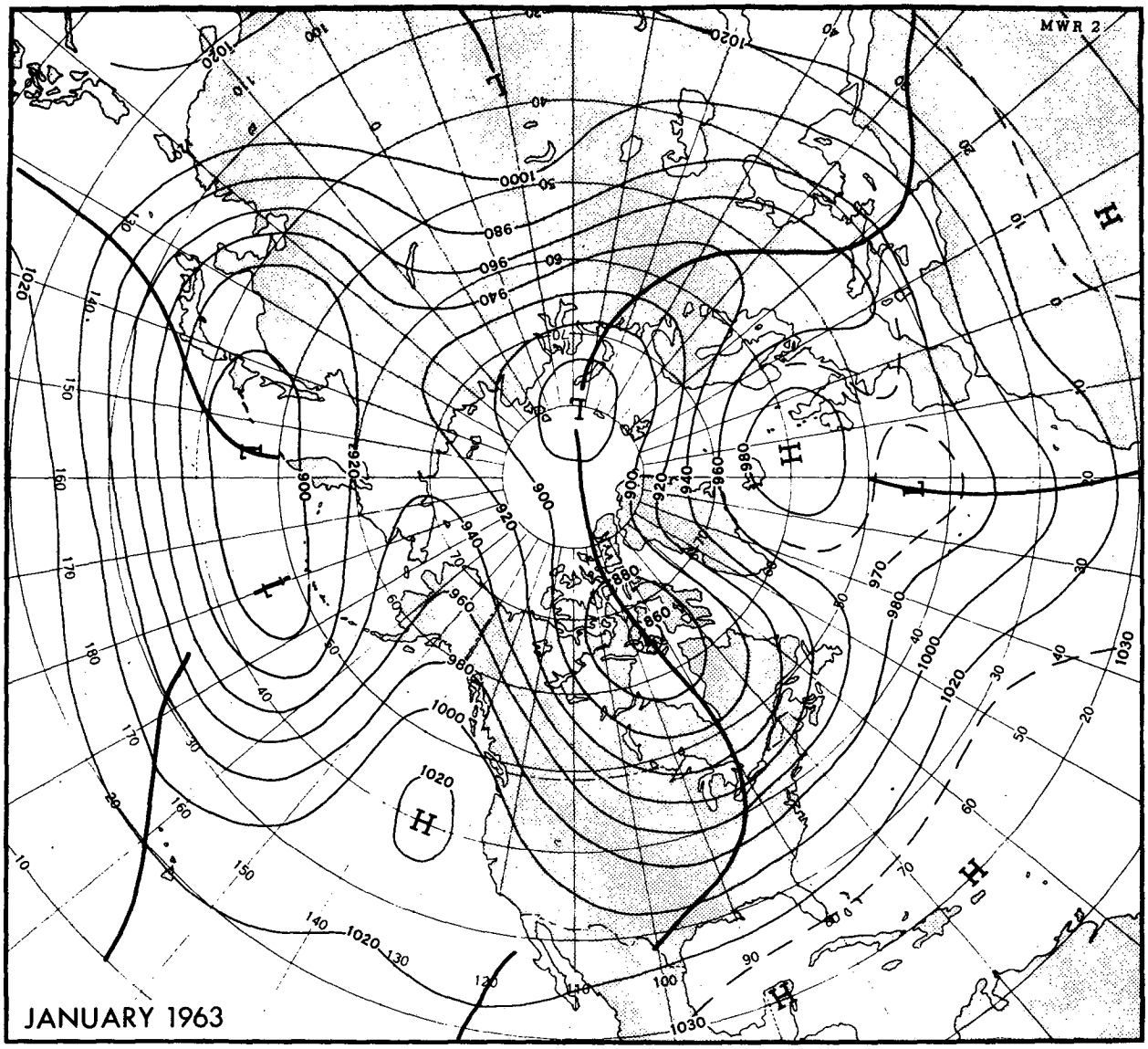

FIG. 13. Average contours of 700 mb surface (tens of feet) for January 1963. Troughs are indicated by solid lines (after O'Connor, 1963).

a. January 1963

1) SYNOPTICS

It was observed that during January 1963 a persistent and amplified ridge existed in the eastern Pacific (O'Connor, 1963). The average circulation at 700 mb is shown in Fig. 13. The pronounced features of the atmospheric circulation in this month were an enormously amplified ridge in the eastern Pacific, a blocking high between Iceland and Britain, and another strong ridge over central Asia. These three ridges were accompanied by an abnormally amplified eastern North American trough, a deep Azores low, a European trough and a Pacific low extending from the west Pacific to Hawaii. Cold Arctic air was brought to northeast North America, Europe and the Far East, while anomalously warm temperatures were experienced over Alaska and Greenland. In addition, most of the trough and ridge lines tilted from southeast to northwest similar to the circulation patterns observed during the persistent blocking episode in the anomaly run.

2) ENERGETICS

The energetics analysis of January 1963 discussed below is based upon the studies of Wiin-Nielsen (1964), Wiin-Nielsen *et al.* (1964) and Murakami and

Tomatsu (1965). The Lorenz energy cycle for this month is shown in Fig. 14c. The directions of energy conversions, $C(A_Z, A_E) = 6.43$ W m^{-2} and $C(A_E, K_E) = 2.96$ W m^{-2}, are the same as conventional studies (Lorenz, 1967). Surprisingly, $C(K_E, K_Z)$ for this month has a large negative value of -1.29 W m^{-2} indicating that the zonal flow was barotropically unstable during this month. This situation is similar to the model anomaly run. The time variations of various energy components in January 1963 are depicted in Figs. 14a and 14b. Note that A_E and K_E increase (decrease) when A_Z and K_Z decrease (increase). The overall picture of the time variation of January 1963 atmospheric energetics shown in Fig. 14 is similar to Lejenäs' during a blocking situation described in Fig. 7. Note that A_Z started to decline and A_E and K_A increased significantly from 10 January on. It is suggested that the January block in 1963 started around this day.

The spectral energetics of January 1963 are displayed in Fig. 15. The spectra of A_n (Fig. 15a), and K_n (Fig. 15b) show that wavenumbers 2 and 3 have the largest values. This may indicate that the atmospheric circulation of this month is mainly described by wavenumbers 2 and 3. It also suggests that the persistent blocking episodes during this particular January were due to the constructive interference of these waves, similar to our model results.

$C(A_n, K_n)$ is extracted from the result of Murakami and Tomatsu (1965). $C(A_Z, A_n)$ (Fig. 15c) and $C(A_n, K_n)$ (Fig. 15e) for wavenumbers 2 and 3 are positive and dominant, while $C(K_3, K_Z)$, shown in Fig. 15d, has a very large negative value of -1.14 W m^{-2}. This negative value of $C(K_3, K_Z)$ indicates that K_3 is maintained by the energy converted from K_Z. Comparing Figs. 15d and 14c, we can see that the energy converted from K_Z to K_3 explains most of the total energy conversion from K_Z to K_E. This shows that wavenumber 3 is barotropically amplified. The discussions above indicate that A_2 and A_3 are maintained by $C(A_Z, A_2)$ and $C(A_Z, A_3)$, respectively. K_2 is maintained by $C(A_2, K_2)$, baroclinic energy conversion, while K_3 is maintained by both $C(A_3, K_3)$ and $-C(K_3, K_Z)$. In other words, a significant component of K_3 is maintained by a barotropic conversion mechanism. The energetics of wavenumbers 2 and 3 in January 1963 are then similar to those in the anomaly run.

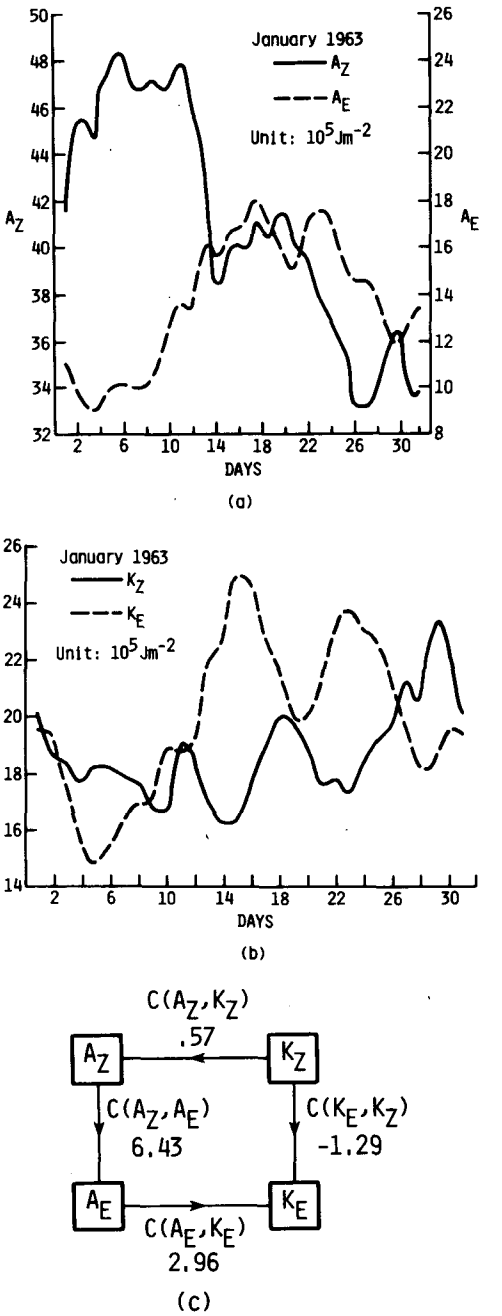

FIG. 14. Energetics for January 1963: (a) time variation of A_Z and A_E, (b) time variation of K_Z and K_E, and (c) Lorenz energy cycle (after Wiin-Nielsen, 1964).

b. January–February 1977

1) SYNOPTICS AND SPECTRAL ANALYSIS

The main features of the atmospheric circulation during the winter of 1976–77 were very persistent through the whole season (Taubensee, 1977; Wagner, 1977; Dickson, 1977). The mean 700 mb circulation for this winter is shown in Fig. 16 (Namias, 1978). Deep troughs persisted over the central Pacific Ocean and eastern North America while a strong persistent blocking ridge was located near the west coast of North America. Warm air was then advected to Alaska by the southerly winds to the west of the ridge, while cold Arctic air, accompanied with heavy snows, was brought to the northeastern sections of the United States. This persistent blocking ridge also caused droughts in the west of this country. The circulation pattern of this winter was characterized by

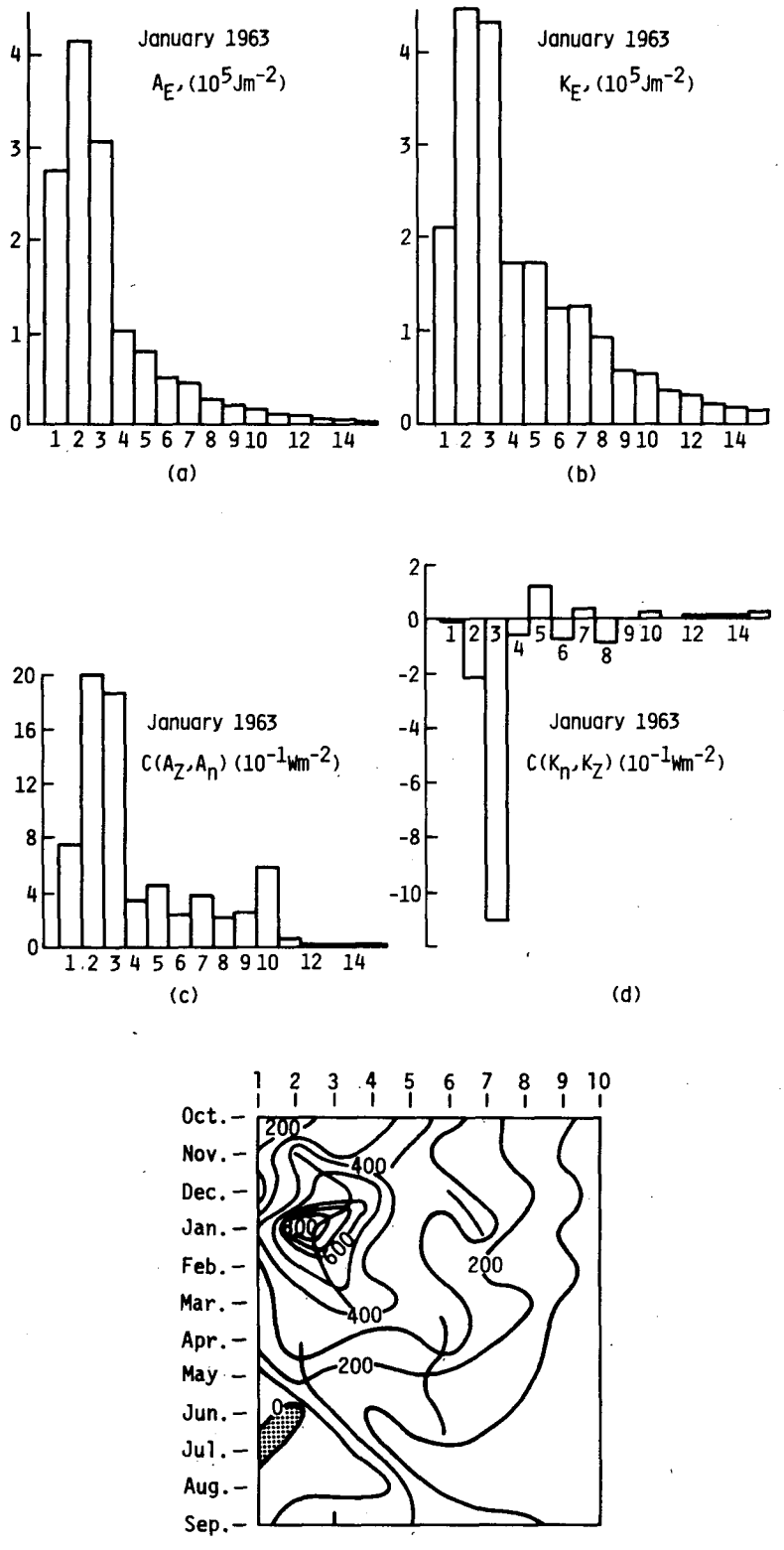

FIG. 15. Spectral energetics for January 1963: (a) A_E spectrum, (b) K_E spectrum, (c) $C(A_Z, A_n)$ spectrum, (d) $C(K_n, K_Z)$ spectrum and (e) $C(A_n, K_n)$ as a function of time (ordinate) and wavenumber (abscissa). These figures are extracted from various studies: (a) and (b) from Wiin-Nielsen *et al.* (1964), and (3) from Murakami and Tomatsu (1965).

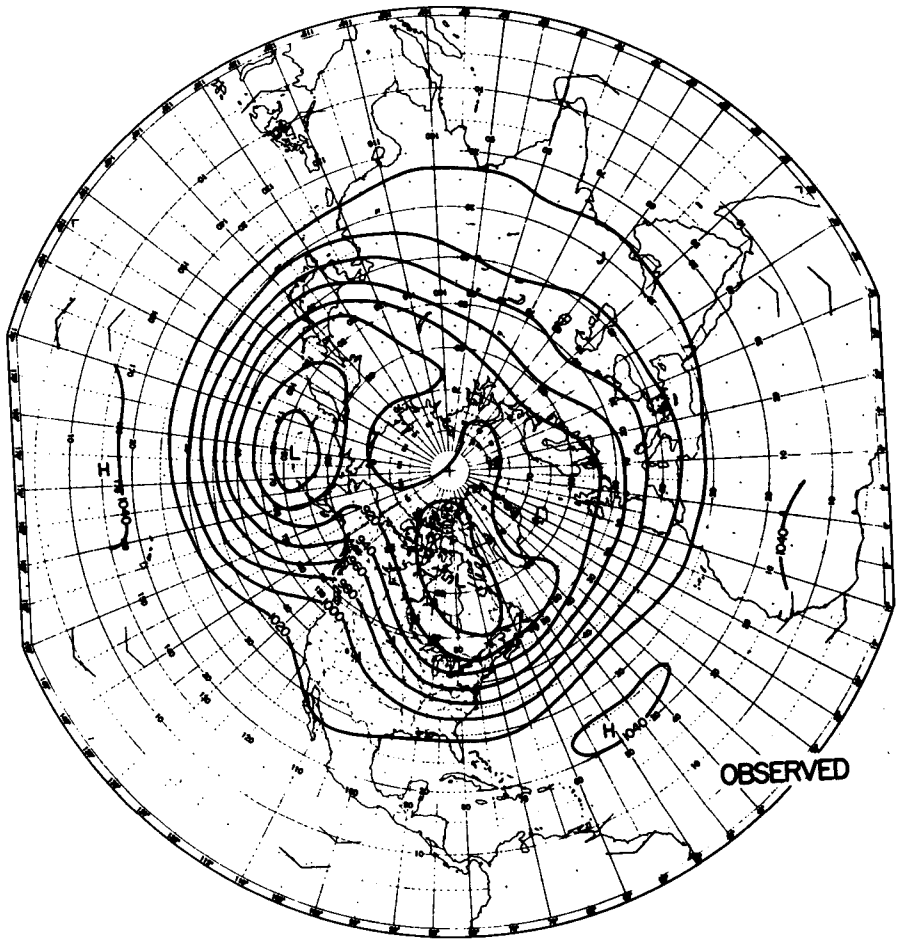

FIG. 16. Mean 700 mb contours (tens of feet) for the winter of 1976–77 (December, January and February) (after Namias, 1978).

the single-block system described above and was different from that of either the anomaly run or January 1963 which had a double-block system.

The spectral analysis of the wave motions are illustrated by the 500 mb SF Hovmöller diagrams at 50°N (Fig. 17a). The total-wave SF Hovmöller diagram presents a very persistent and strong narrow blocking ridge between 90 and 150°W and a broad weak climatological ridge between 30°W and 90°E. The strong narrow blocking ridge between 90 and 150°W existed since the first week of January 1977 and before, and decayed at the end of the third week of February. Comparing Figs. 17a and 17b, we again see that the long waves explain the major features of the blocking ridges as in the anomaly run and the January 1963 case. The short-wave SF Hovmöller diagram shows that the synoptic-scale waves generally propagate steadily eastward, except between 120°W and 120°E, i.e., over the Pacific, where the short-wave ridges and troughs become quasi-stationary. Namias (1978) claimed that the significant west–east Pacific SST gradient enhanced the cyclogenesis and the upper-level southerlies which steered the storm northward. The existence of quasi-stationary short-wave ridges and troughs may indicate that the cyclogenesis occurs in the same areas very often or that the storms simply change direction here. This feature is also found in the anomaly run.

The SF Hovmöller diagrams of individual waves are also displayed in Figs. 17d–h. All the long waves (n = 1–4), during January–February 1977 at 50°N, were quasi-stationary. The locations of these long-wave ridges are very close to those shown in Eliasen's (1958) study (also displayed in Fig. 1 of Austin, 1980) for the climatology of these long waves. It is also of interest to note that the strong narrow blocking ridge between 90 and 150°W (Fig. 17a or 17b) decayed when wavenumbers 3 and 4 weakened and became eastward propagating in the last week of February.

We now compare the SF Hovmöller diagrams of the individual long waves in the anomaly run (Fig. 3) with those during January–February 1977. The

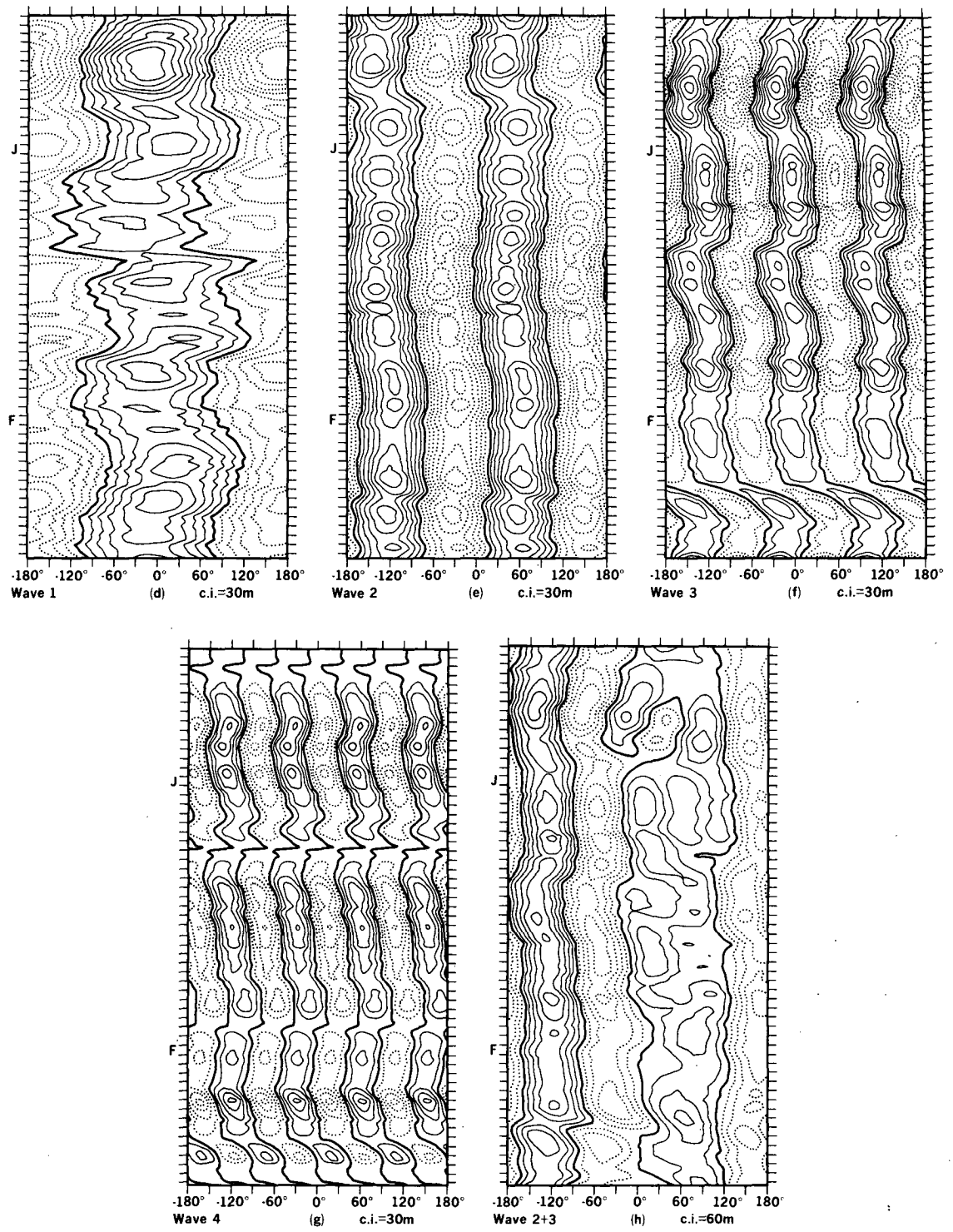

FIG. 17. Spectrally filtered Hovmöller diagrams of various waves at 500 mb and 50°N for January–February 1977.

ridge of model wavenumber 1 is located around 60°W at the onset of the model block. This ridge location is west of the 0° longitude wavenumber 1 ridge position as determined climatologically from atmospheric data. When wavenumbers 2 and 3 become stationary in the anomaly run the ridge positions of these two waves are very close to the observations. Wavenumber 4 is an essentially eastward

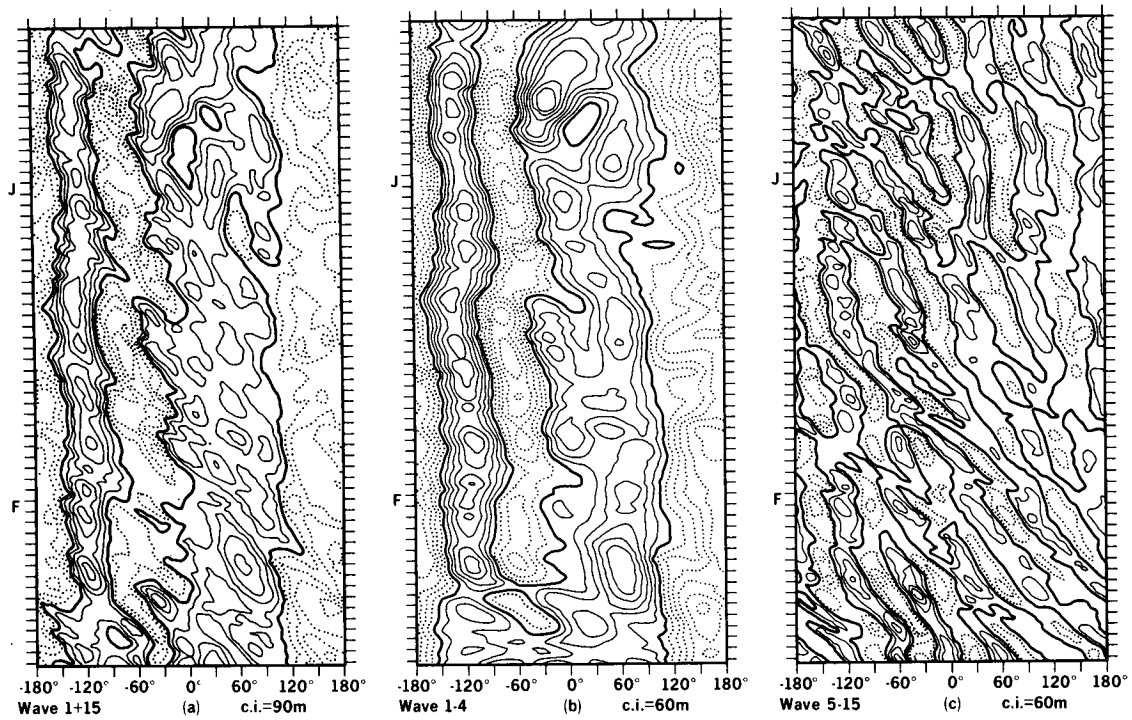

FIG. 17. (*Continued*)

moving wave in the anomaly run. These comparisons show that the characteristics of wavenumbers 1 and 4 in the anomaly run are different from those in the winter of 1976–77. Although the constructive interference of wavenumbers 2 and 3 in this winter can form the blocking ridge over the west coast of North America (Fig. 17h), as in the anomaly run, the quasi-stationary nature of wavenumbers 1 and 4 in the winter of 1976–77 makes their contribution to the formation of the blocking ridge impossible to be ruled out.

2) ENERGETICS

We have used observational data analyzed by the National Meteorological Center (NMC) and archived at the National Center for Atmospheric Research (NCAR) to examine the spectral energetics of the 1976–77 winter. The region of integration covers 30–80°N. The ω fields, which were used to calculate $C(A_E, K_E)$, were evaluated by the scheme proposed by Chen *et al.* (1981). The energetics computations for January–February 1977 reveal that time variations of A_E and K_E were not very significant, and A_Z and K_Z increased somewhat in February (not shown). The slight enhancement of A_Z and K_Z is due to the breakdown of the blocking ridge in later February shown in Fig. 17a. This figure also shows that an Atlantic block existed in the first 10 days of January. Time variations of various energy terms during this period are the same as Lejenäs' schematic diagram.

The Lorenz energy cycle of these two months is depicted in Fig. 18. The directions of various energy conversions are the same as those seen in conventional studies. However a remarkable difference between the energy cycle of January–February 1977 and that of the anomaly run is that $C(K_E, K_Z)$ is of opposite sign. In other words, the eddies during this winter were barotropically stable. In addition, Rosen and Salstein (1980) pointed out that the 1976–77 winter had strong $C(K_E, K_Z)$. Note that $C(K_E, K_Z)$ is evaluated with the covariance of eddy momentum transport and north–south horizontal gradient of zonal flow. These two variables are much larger during this winter (as observed by Rosen and Salstein), and, in turn, explain why $C(K_E, K_Z)$ has a larger value than a normal winter.

The spectral energetics of January–February 1977 are displayed in Fig. 19. A_3 is somewhat smaller than A_1 and A_2, but K_3 is comparable to K_1. Let us recall the SF Hovmöller diagrams discussed above indicate that the formation of the blocking ridge in this winter is different from the anomaly run. In order to compare the spectral energetics of this winter with that of the anomaly run, we shall focus on wavenumbers 2 and 3 whose constructive interference forms the blocking ridges in the anomaly run. $C(A_Z, A_2)$ and $C(A_Z, A_3)$ dominate $C(A_Z, A_E)$ and are the sources which supply A_2 and A_3, respectively. K_2 and K_3 are maintained by $C(A_2, K_2)$ and $C(A_3, K_3)$, respectively, and $C(K_2, K_Z)$ is quite small compared to $C(A_2, K_2)$.

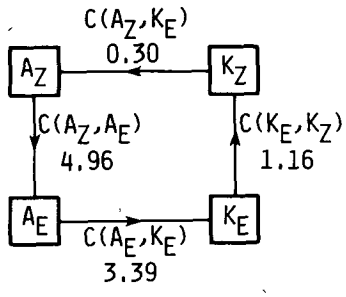

FIG. 18. Energy cycle (W m^{-2}) for January–February 1977.

However, the significant nonlinear interaction $CK(2|m, l)$, shown in Fig. 19g, seems to absorb the supply to K_2 by $C(A_2, K_2)$. On the other hand, K_3 is substantially depleted by $C(K_3, K_Z)$, which is even more significant in view of the fact that $C(K_3, K_Z)$ explains 45% of $C(K_E, K_Z)$.

The spectral energetics of the 1976–77 winter discussed so far shows clearly that wavenumbers 2 and 3 are maintained by the baroclinic process. The depletion of K_2 is mainly due to nonlinear transfers, while K_3 is due to the barotropic process, $C(K_3, K_Z)$. It is obvious that the energetics of these two waves are different from the anomaly run in which wavenumber 2 is maintained by baroclinic conversion and wavenumber 3 by barotropic conversion.

6. Summary

A blocking event was generated in the GLAS climate model by imposing the sea surface temperature (SST) anomalies which had the same spatial structure as observed by Namias (1978) but of greater amplitude by a factor of 9/5. The major effort of this study is to examine the spectral characteristics and energetics of this blocking event. It is found that wavenumbers 2 and 3 became stationary around their climatological locations. The constructive interference of wavenumbers 2 and 3 forms two persistent blocking ridges: one over the west coast of North America and the other over western Europe.

The total energy budget analysis shows that the time variations of A_Z, A_E, K_Z, K_E, and energy conversions during the model blocking episode are similar to a typical blocking situation as defined and analyzed by Lejenäs (1977). Spectral energetics of wavenumbers 2 and 3 shows that A_2 and A_3 are maintained by $C(A_Z, A_2)$ and $C(A_Z, A_3)$, respectively. K_2 is maintained by $C(A_2, K_2)$, the baroclinic energy conversion from A_2 to K_2, $C(A_Z, A_2)$, while K_3 is maintained by the barotropic energy conversion from K_2 to K_3, $-C(K_3, K_Z)$.

The abnormal circulation patterns and severe weather conditions in both January 1963 and the 1976–77 winter were similar to some extent, especially in the sense that there was a persistent and enormously amplified ridge over the west coast of North America (as in the anomaly run). Note that some synoptic difference exists between these two winters: lack of a "double" block in the 1976–77 winter. However, effort was made in this study to compare the spectral analyses and energetics between these two winters and the anomaly run with the hope that we may gain further understanding about the physical mechanisms causing and maintaining the persistent blocking ridges.

The spectrally filtered Hovmöller diagrams for the 1976–77 winter show that all the long waves (n = 1–4) are stationary over most of this time period. The blocking ridge located in the west coast of North America in this winter was formed by the constructive interference of these long waves, especially wavenumbers 2 and 3. The blocking ridge decayed when wavenumbers 3 and 4 started to move eastward. Apparently, the kinematic formation of the blocking ridge in the 1976–1977 winter is different from the anomaly run. This difference would be due to the different synoptic structure in this winter as described above. The spectral energetics of January 1963 analyzed by Wiin-Nielsen (1964), Wiin-Nielsen *et al.* (1964) and Murakami and Tomatsu (1965) show that the energetics of wavenumber 2 and 3 are similar to the anomaly run. In particular, wavenumber 3 was vitally maintained by the barotropic energy conversion from K_Z to K_3 while wavenumber 2 was maintained by baroclinic processes. On the other hand, the development and maintenance of wavenumbers 2 and 3 in the 1976–77 winter is different from either January 1963 or the anomaly run in the sense that K_3 is depleted significantly by the barotropic energy conversion about K_3 to K_Z.

Egger (1978) and Kalnay-Rivas and Merkine (1981) proposed that blocking can be caused by a barotropic mechanism, while Schilling (1982) shows, on the other hand, that the blocking can be induced by a baroclinic mechanism. However, these studies only use simple models to test their proposals. The present study has shown that the double blocks which appeared in the anomaly run and January 1963 were essentially formed by the constructive interference of wavenumbers 2 and 3. The maintenance of these two waves appears to be scale-selective in the fact that wavenumber 2 is maintained by baroclinic processes and wavenumber 3 by barotropic processes. It indicates that neither the baroclinic nor barotropic mechanism alone can be responsible for the formation and maintenance of blockings in the atmosphere or sophisticated general circulation model.

Finally, an interesting question is raised as to why the dynamical processes that maintain the blocking ridge in January 1963 and the anomaly run is scale-selective. The answer is beyond the scope of the present study. Nevertheless, it would be of interest to

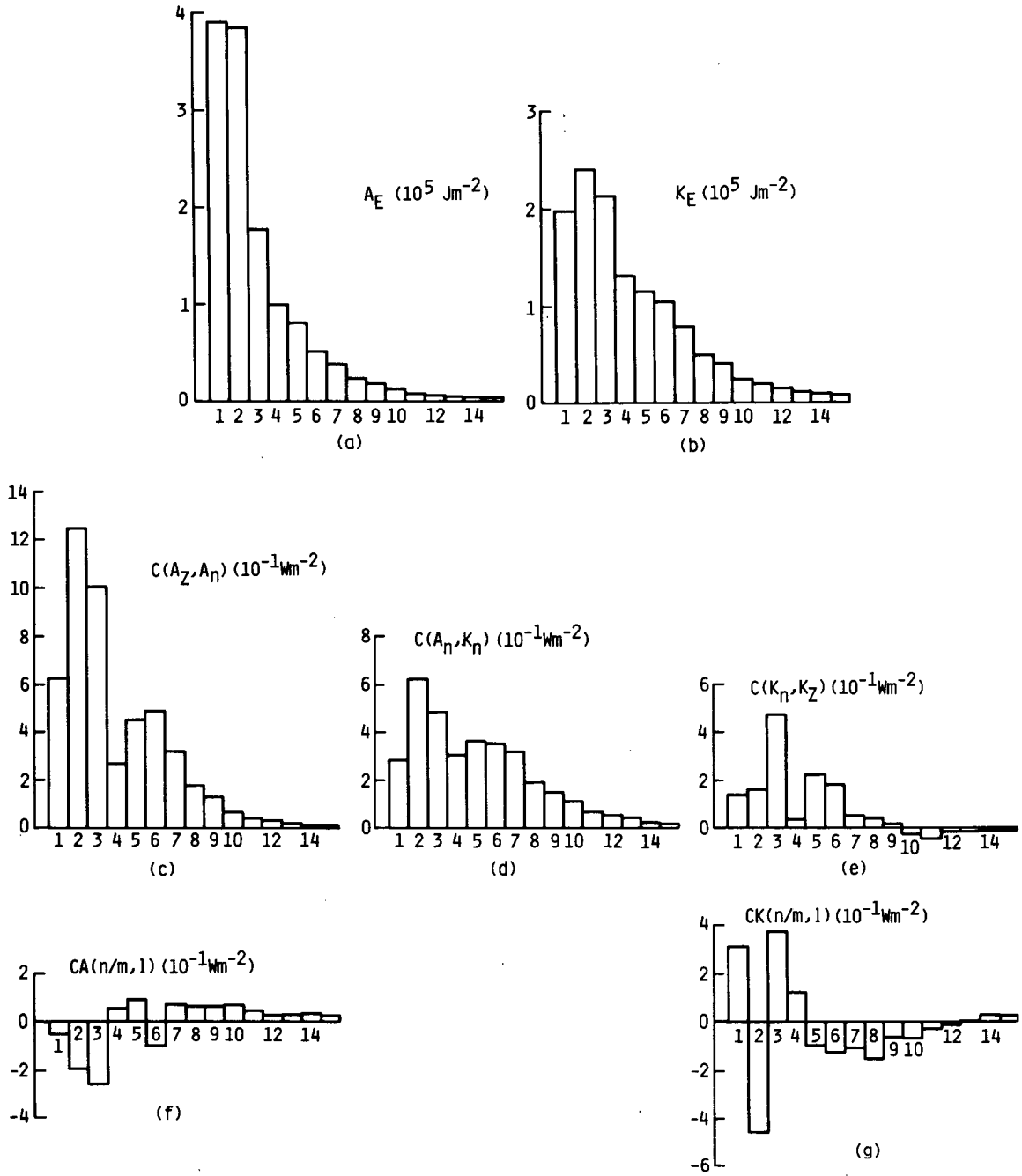

FIG. 19. Spectral energetics for January–February 1977: (a) A_E spectrum, (b) K_E spectrum, (c) $C(A_Z, A_n)$ spectrum, (d) $C(A_n, K_n)$ spectrum, (e) $C(K_n, K_Z)$ spectrum, (f) $CA(N|m, l)$ and (g) $CK(n|m, l)$.

make further examinations of other blocking cases and perhaps ascertain whether the double blocking situation (as present in our two cases) is consistently maintained by a similar scale-selective dynamical process.

Acknowledgments. The help and effort provided by Mr. Hal Marshall and Mr. J. E. Nielsen made this study possible. We are also grateful for the reviewer's critical comments which led to substantial improvement of this paper. This study is supported by the NASA Grants NSG-4339 and NAG5-104.

REFERENCES

Austin, J. R., 1980: The blocking of middle latitude westerly winds by planetary waves. *Quart. J. Roy. Meteor. Soc.*, **106**, 327–350.

Bengtsson, L., 1981: Numerical prediction of atmospheric blocking—A case study. *Tellus*, **33**, 19–42.

Chen, T.-C., 1982: A further study of spectral energetics in the winter atmosphere. *Mon. Wea. Rev.*, **110**, 947–961.

——, A. R. Hansen and J. J. Tribbia, 1981: A note on the release of available potential energy. *J. Meteor. Soc. Japan*, **59**, 355–360.

Dickson, R. R., 1977: Weather and Circulation of February 1977—Widespread drought. *Mon. Wea. Rev.*, **105**, 684–689.

Egger, J., 1978: Dynamics of blocking highs. *J. Atmos. Sci.*, **35**, 1788–1801.

Eliasen, E., 1958: A study of the long atmospheric waves on the basis of zonal harmonic analysis. *Tellus*, **10**, 206–215.

Halem, M., J. Shukla, Y. Mintz, M. L. Wu, R. Godbale, G. Herman and Y. Sud, 1979: Comparisons of observed seasonal climate features with a winter and summer numerical simulation produced with the GLAS general circulation model. Report of the JOC Study Conf. on Climate Models: Performance, Intercomparison and Density Studies, *GARP Publ. Ser.*, No. 22, 207–253, WMO, Geneva.

Hansen, A. R., and T.-C. Chen, 1982: A spectral energetics analysis of atmospheric blocking. *Mon. Wea. Rev.*, **110**, 1146–1165.

Hovmöller, E., 1949: The trough-and-ridge diagram. *Tellus*, **1**, 62–66.

Kalnay-Rivas, E., and Lee-Or Merkine, 1981: A simple mechanism for blocking. *J. Atmos. Sci.*, **38**, 2077–2091.

Lejenäs, H., 1977: On the breakdown of the westerlies. *Atmosphere*, **15**, 89–113.

Lorenz, E. N., 1967: The nature and theory of the general circulation of the atmosphere. Tech. Note No. 218, TP115, WMO, Geneva, 161 pp.

Miyakoda, K., 1963: Some characteristic features of winter circulation in the troposphere and the lower stratosphere. University of Chicago Tech. Rep. No. 14 [Available from Photoduplication Dept., Library of the University of Chicago, Chicago, IL, 60637].

Murakami, T., and K. Tomatsu, 1965: Energy cycle in the lower atmosphere. *J. Meteor. Soc. Japan*, **43**, 73–89.

Namias, J., 1970: Macroscale variations in sea-surface temperatures in the North Pacific. *J. Geophys. Res.*, **75**, 565–582.

——, 1978: Multiple causes of the North American abnormal winter 1976–1977. *Mon. Wea. Rev.*, **106**, 279–295.

O'Connor, J. F., 1963: The Weather and Circulation of January 1963. *Mon. Wea. Rev.*, **91**, 209–218.

Paulin, G., 1970: A study of the energetics of January 1959. *Mon. Wea. Rev.*, **98**, 795–809.

Rosen, R. D., and D. A. Salstein, 1980: A comparison between circulation statistics computed from conventional data and NMC Hough analysis. *Mon. Wea. Rev.*, **108**, 1226–1247.

Saltzman, B., 1957: Equations governing the energetics of the larger scales of atmospheric turbulence in the domain of wavenumber. *J. Meteor.*, **14**, 513–523.

Schilling, H.-D., 1982: A numerical investigation of the dynamics of blocking waves in a simple two-level model. *J. Atmos. Sci.*, **39**, 998–1017.

Shukla, J., and B. Bangaru, 1979: Effect of a pacific sea surface temperature anomaly on the circulation over North America. *Fourth National Aeronautics and Space Administration Weather and Climate Program Science Review*, the NASA Goddard Space Flight Center, Greenbelt, MD, 20771, 171–176.

Starr, V. P., 1948: An essay on the general circulation of the earth's atmosphere. *J. Meteor.*, **2**, 39–43.

Steinberg, H. L., A. Wiin-Nielsen and C.-H. Yang, 1971: On nonlinear cascades in large-scale atmospheric flow. *J. Geophys. Res.*, **76**, 8629–8640.

Taubensee, R. E., 1977: Weather and Circulation of December 1976. *Mon. Wea. Rev.*, **105**, 368–373.

Tung, K. K., and R. S. Lindzen, 1979: A theory of stationary long waves. Part I: A simple theory of blocking. *Mon. Wea. Rev.*, **107**, 714–734.

Wagner, A. J., 1977: Weather and Circulation of January 1977. *Mon. Wea. Rev.*, **105**, 553–560.

Wiin-Nielsen, A., 1964: Some new observational studies of energy and energy transformations in the atmosphere. Tech. Note No. 66, WMO, Geneva, 177–202.

——, J. A. Brown and M. Drake, 1964: Further studies of energy exchange between the zonal flow and eddies. *Tellus*, **16**, 168–180.

Winston, J. S., and A. F. Krueger, 1961: Some aspects of a cycle of available potential energy. *Mon. Wea. Rev.*, **89**, 307–318.